Evolution of activation energies for hot deformation of 7150 aluminum alloys with various Zr and V additions

Cangji Shi, X.-Grant Chen *

Department of Applied Science, University of Québec at Chicoutimi,
Saguenay (QC), Canada G7H 2B1

Abstract

The flow stress behavior of 7150 aluminum alloys with different Zr (0 to 0.15 wt%) and V (0.01 to 0.15 wt%) additions was investigated using uniaxial compression tests conducted at various temperatures and strain rates. Using revised Sellars' constitutive analysis, the activation energy maps for hot deformation of 7150 alloys are proposed, which are considered as a function of deformation temperature, strain rate and micro-alloying elements. The results reveal that the activation energies of all 7150 alloys decrease with increasing deformation temperature and increasing strain rate. The activation energies for hot deformation of the alloy with 0.12-0.15% Zr are remarkably increased compared to those of the base alloy at most deformation conditions, due to the pinning effect of Al_3Zr dispersoids on dislocation and the restrained dynamic recovery. The 0.05% V addition significantly increases activation energies, preferentially at lower temperatures of 573-623 K, correlated with V solute drag effect. At higher V additions from 0.11 to 0.15%, the activation energy generally increases at the majority of deformation conditions due to $Al_{21}V_2$ dispersoid pinning effect. However, remarkable decreases in activation energy exhibit at low deformation temperatures of 573-700 K and at low strain rates of 0.001-0.008 s^{-1}, attributed to the enhanced dynamical precipitation and severe depletion of solutes. Comparing the activation energy maps for the alloys studied, the effects of micro-alloying of Zr and V on the plastic deformation under specific deformation conditions can be better understood.

Keywords: 7150 aluminum alloy, Zr and V additions, Constitutive equations, Activation energy, Dispersion pinning effect, Solute drag effect.

* Corresponding author:
Department of Applied Science, University of Québec at Chicoutimi
Saguenay (QC), Canada G7H 2B1
Tel.: 1-418-545 5011 ext. 2603; Fax: 1-418-545 5012
E-mail: xgrant_chen@uqac.ca

1. Introduction

Due to a high strength-to-density ratio and excellent mechanical fracture toughness, 7150 aluminum alloys (Al-Zn-Mg-Cu) have been widely used in aircraft structure components [1]. These aluminum alloys are generally subjected to hot forming processes such as rolling, forging and extrusion. The mechanical properties are closely related to the microstructures, which are greatly influenced by the alloying elements and thermomechanical factors, such as deformation temperature, strain rate and strain [2-6]. Dynamic recovery and dynamic recrystallization during the hot deformation result in the complex microstructural evolution and simultaneously affect the plastic deformation behaviors [2,7]. Understanding of the effects of micro-alloying and thermomechanical processing on high temperature deformation behavior is important for the design of hot forming processes to improve the mechanical properties of products.

The addition of zirconium is well known to increase the recrystallization resistance of aluminum alloys by forming fine, coherent Al_3Zr dispersoids [4,8]. The presence of the Al_3Zr dispersoids promotes the formation of a stable and refined subgrain structure during the hot working, which promotes additional substructure strengthening [9]. Vanadium addition is reported to maintain high temperature strength of the aluminum alloy by forming thermally stable dispersoids of $Al_{11}V$ [10,11]. Those dispersoids could retard dynamic softening and raise recrystallization temperature during hot working processes [12]. The effectiveness of the dispersoids depends on their size, number density and distribution [7].

The constitutive relation is generally established to describe the relationship between the flow stress and thermomechanical factors. Several constitutive models have been proposed, including physical-based, phenomenological and artificial neural network models and equations [13]. Among all, the hyperbolic-sine law, proposed by Sellars and McTegart [14], has been proven to be most applicable over a wide range of stresses. The activation energy of a material for hot deformation derived from this relation is usually used as an indicator of the degree of difficulty of the hot deformation process. Cerri et al. [15] reported that deformation activation energies for the precipitated and over aged 7012 aluminum alloys are 141-162 kJ/mol, similar to that of pure aluminum, 142 kJ/mol. Jin et al. [16] reported the activation energy for homogenized 7150 aluminum alloy is 229.75 kJ/mol, which is higher than the aged 7150 alloy (158.8-161.4 kJ/mol) [17], and close to the values of the solution-treated 7012 alloy (200–230 kJ/mol) [15] and the as-quenched 7050 alloy (256.6 kJ/mol) [18]. In the author's recent works [19,20], it is found that the hot deformation activation energy of the 7150 alloys increases progressively with increasing Zr addition and reaches 255.2 kJ/mol when being alloyed with 0.19% Zr. In addition, the 7150 alloys containing 0.03-0.05% V display high activation energies, approximately 270 kJ/mol. With a further increase in V content up to 0.19%, the activation energy achieves approximately 250 kJ/mol.

In the majority of research [13-20], the activation energy has been treated as a constant value for all applied hot deformation conditions. However, the activation energy for hot deformation represents the free energy barrier to dislocation slipping, which is affected by the temperature, external stress and microstructure during hot-forming processes [2,21]. A revised Sellars' constitutive equation was proposed by Shi et al. [22], which considered the effects of deformation temperature and strain rate on

the material variables. However, under different deformation conditions, the effects of alloying elements on the evolution of activation energy for hot deformation have rarely been reported.

In the present paper, the hot deformation behavior of 7150 alloys with different Zr and V additions is studied using hot compression tests performed at various temperatures and strain rates. Using revised Sellars' constitutive analysis, the activation energy maps for hot deformation of 7150 alloys are proposed. The effects of Zr and V micro-alloying on activation energy maps under various deformation conditions are investigated. The thermodynamic mechanism of the evolution of activation energy is discussed.

2. Experimental

Experiments were conducted on 7150 base alloy and alloys with different Zr contents from 0.04 to 0.15% and V contents from 0.05 to 0.15% (all alloy compositions are in wt% unless otherwise indicated). The chemical compositions of those alloys are provided in Table 1. Approximately 3 kg of each material was melted in an electrical resistance furnace and then cast into a rectangular permanent steel mold measuring 30 x 40 x 80 mm^3. The cast ingots of these alloys were homogenized at 465 °C for 24 h, followed by direct water quenching to room temperature. Cylindrical samples measuring 10 mm in diameter and 15 mm long were machined from the homogenized ingots. Uniaxial compression tests were conducted on a Gleeble 3800 thermomechanical simulation unit at strain rates of 0.001, 0.01, 0.1, 1 and 10 s^{-1} and deformation temperatures of 300, 350, 400 and 450 °C, respectively. During the tests on the Gleeble 3800 unit, the samples were heated to the desirable deformation temperature at a heating rate of 10 °C/s and held for 3 min to ensure a homogeneous temperature distribution throughout the samples. The samples were deformed to a total true strain of 0.8 and then immediately water-quenched to retain the microstructure at the deformation temperature.

The microstructure of the as-homogenized materials was etched by Keller's solution prior to hot deformation. Additionally, some deformed samples were selected for electron backscattered diffraction (EBSD) analysis under a scanning electron microscope (SEM, JEOL JSM-6480LV). The step size between the scanning points was set to 1.0 μm. Samples for TEM observation were mechanically ground to a thicknesses of 35-60 μm and followed by electropolishing in a twin-jet polishing unit, which was operated at 15 V and -20 °C using a 30% nitric acid and 70% methanol solution. The samples were observed under a transmission electron microscope (TEM, JEOL JEM-2100) operated at 200 kV. The thickness of the TEM sample was determined via electron energy loss spectroscopy (EELS). Precipitate size and volume fraction were quantitatively measured using an image analyzer (CLEMEX JS-2000, software PE7.0) [23].

Table 1 Chemical composition of the alloys studied (wt%).

Alloy	Zn	Mg	Cu	Si	Fe	Ti	Zr	V	Al
Base alloy	6.44	2.47	2.29	0.16	0.15	0.009	-	0.01	Bal.
With 0.04%Zr	6.27	2.14	2.23	0.11	0.14	0.008	0.04	0.01	Bal.
With 0.12%Zr	6.35	2.22	2.34	0.16	0.15	0.008	0.12	0.01	Bal.
With 0.15%Zr	6.16	2.15	2.16	0.11	0.14	0.008	0.15	0.01	Bal.

With 0.05%V	6.21	2.18	2.20	0.16	0.14	0.009	-	0.05	Bal.
With 0.11%V	6.31	2.30	2.24	0.16	0.14	0.008	-	0.11	Bal.
With 0.15%V	6.16	2.10	2.15	0.16	0.13	0.008	-	0.15	Bal.

3. Results

3.1 Flow stress behavior

Fig. 1 shows the typical flow stress curves obtained during hot compression for the 7150 aluminum alloys containing Zr from 0 to 0.15% and V from 0.01 to 0.15% under different deformation conditions. For all those alloys, the flow stresses increase rapidly at the initial stage of deformation and then either keep fairly constant or decrease to some extent after attaining a peak stress. The flow stress level decreases with increasing deformation temperature and with decreasing strain rate. Under any given deformation condition, the alloy containing 0.04% Zr exhibits a similar value in flow stress compared with the base alloy. With increasing Zr contents from 0.12 to 0.15%, the flow stress gradually rises. On the other hand, the alloy with 0.05% V addition displays remarkable increases in flow stress relative to the base alloy at the same deformation conditions, especially at low deformation temperatures between 573 and 623 K. As the V content further increases from 0.11 to 0.15%, the flow stress levels are improved significantly at all temperature ranges studied. Furthermore, it is observed that the micro-alloying of V results in higher values of flow stress compared with the same level of Zr addition at any given deformation condition. Therefore, the additions of Zr and V could enhance the deformation resistance of the base alloy during hot deformation process.

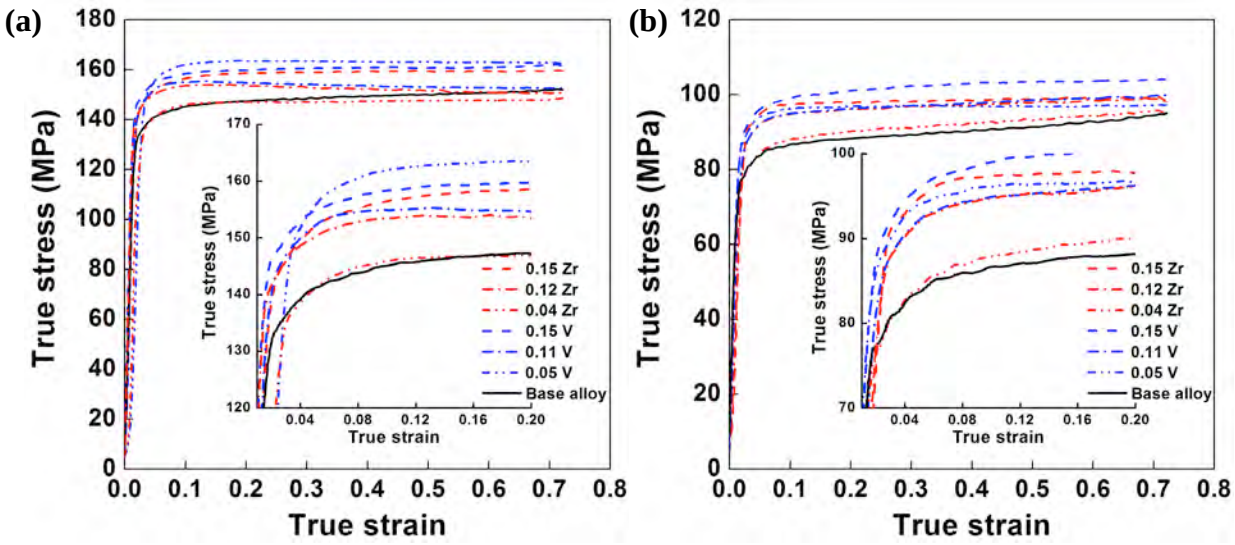

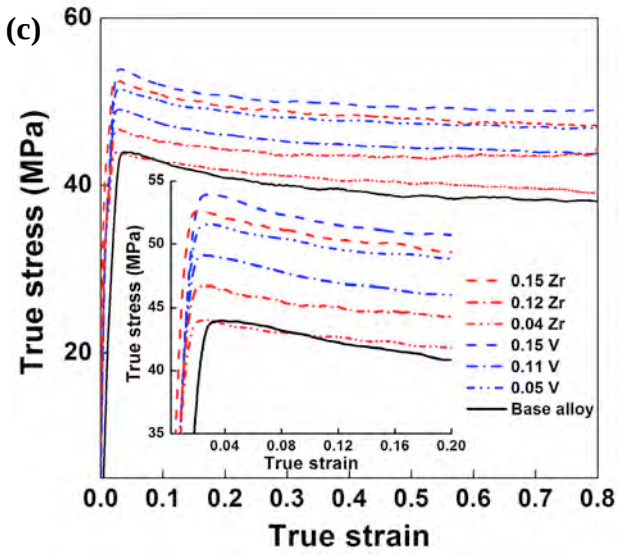

Fig. 1. Typical true stress-true strain curves of 7150 base alloy and alloys with 0.04-0.15% Zr and 0.05-0.15% V under deformation conditions at (a) T=573 K and $\dot{\varepsilon}$ =1 s^{-1}; (b) T=673 K and $\dot{\varepsilon}$ =1 s^{-1} and (c) T=673 K and $\dot{\varepsilon}$ =0.01 s^{-1}.

3.2 Evolution of activation energy for hot deformation

Sellars' constitutive equation

The physical-based hyperbolic-sine equation, proposed by Sellars and McTegart [14], has been widely used to model the relationship between the strain rate, deformation temperature and flow stress of the materials, especially over a wide range of stresses,

$$\dot{\varepsilon} = A[\sinh(\alpha\sigma_p)]^n \exp(-\frac{Q}{RT}) \quad (1)$$

where, n and A are material constants, α is the stress multiplier, σ_p is the peak flow stress (MPa), Q is the activation energy for hot deformation (kJ/mol), R is the universal gas constant (8.314 J/mol K), and T is the deformation temperature (K).

The activation energy for hot deformation, Q derived from Eq. (1) is an important physical parameter serving as an indicator of the degree of difficulty of plastic deformation. In the original Sellars' equation, n, A and the activation energy Q are considered to be material constants which are independent of the deformation conditions (T and $\dot{\varepsilon}$).

Based on the original Sellars' equation and the complete experimental dataset obtained from the true stress-true stain curves at different deformation conditions, the activation energies of the 7150 alloys with different Zr and V additions were calculated [19,20] and are presented in Fig. 2. The activation energy of 229.4 kJ/mol obtained for the 7150 base alloy is in general agreement with the values reported for similar alloys, such as 7050 and 7075 alloys [15,16]. The alloy containing 0.04% Zr exhibits a similar but slightly lower value of 226.5 kJ/mol compared to the base alloy. With increasing Zr content from 0.12 to 0.15%, the Q shows an increased tendency and reaches 255 kJ/mol for the

alloy containing 0.15% Zr. Conversely, the alloy with 0.05% V displays a remarkable increase in activation energy, reaching 272 kJ/mol. As the V content increases from 0.11 to 0.15%, the Q returns to the level of approximately 250 kJ/mol, which still displays higher values relative to the base alloy. By comparison of the activation energy values of these alloys, we can only get a general conclusion, namely that the micro-alloying of Zr and the V considerably increases the difficulty of plastic deformation of the 7150 alloy. However, the variations in deformation resistance at different deformation conditions are still unknown. In addition, the effects of alloying elements on deformation resistance under specific deformation conditions are not clear.

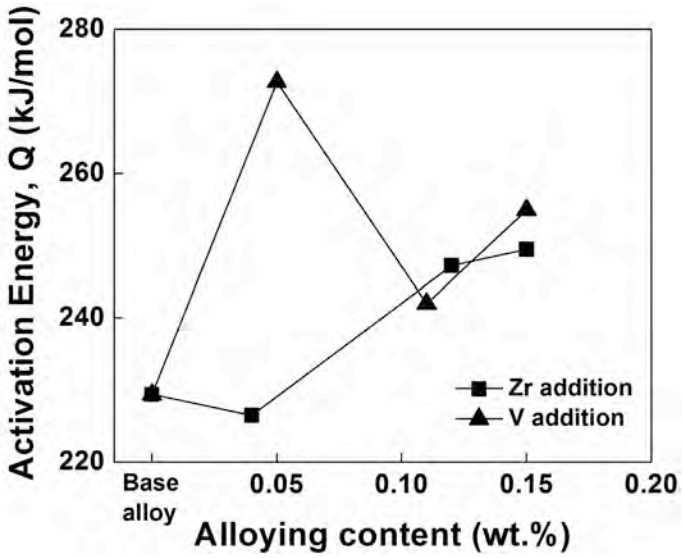

Fig. 2. Evolution of the activation energy for hot deformation of 7150 aluminum alloys as a function of Zr and V content.

In fact, the values of n and A were observed to vary with the deformation temperature or strain rate in our previous studies [19,20,22] and other research works [13-18]. Moreover, the hot deformation of aluminum alloys occurs mainly by dislocation slipping, which is a thermally activated process [2,21]. The activation energy of dislocation slips is reduced by applied external stress, and the deformation resistance is affected by temperature [21]. The variation in the activation energy with temperature and applied stress has been reported during creep of high-purity aluminum and Ni-2vol.% ThO_2 [24,25]. It is obvious that hot deformation process involves dislocation slip, and the effects of thermomechanical factors on the evolution of the activation energy should be considered. Therefore, the original Sellars' equation (Eq. (1)) cannot adequately represent the hot deformation behavior of aluminum alloys.

Revised Sellars' constitutive equation

To overcome the shortcomings of the original Sellars' equation, a revised Sellars' constitutive equation has been proposed in our previous study [22, 26-Shi_TMS 2015] and is given in Eq. (2). Eq. (2) considers the effects of the deformation temperature and strain rate on the material variables and

activation energy. In the present study, to investigate the effects of micro-alloying of Zr and V on the activation energy under various deformation conditions, seven alloys including the base alloy (Table 1) were selected and the evolution of activation energy is evaluated based on Eq. (2).

$$\dot{\varepsilon} = A(T,\dot{\varepsilon})[\sinh(\alpha\sigma_p)]^{n(T)} \exp(-\frac{Q(T,\dot{\varepsilon})}{RT}) \quad (2)$$

where, the material variables n, A and activation energy Q are functions of the deformation temperature and the strain rate.

The experimental dataset obtained for the alloy containing 0.15% Zr are used as an example to derive the values of activation energy Q under different deformation conditions for all materials studied. The data obtained at a strain rate of 10 s^{-1} were not taken into account due to the flow instability leading to a significant rise in deformation temperature [19,20,26]. The stress multiplier α can be defined as $\alpha = \beta / n_1$ [14], where β and n_1 are evaluated from the slopes of the plots of $\ln(\dot{\varepsilon})$ - σ_p and $\ln(\dot{\varepsilon})$ - $\ln(\sigma_p)$, respectively, for the range of temperatures studied. Hence, the value of α for the alloy with 0.15% Zr is determined to be 0.01.

Taking the natural logarithm of both sides of Eq. (2), it yields [22],

$$\ln\dot{\varepsilon} = [\ln A(T,\dot{\varepsilon}) - \frac{Q(T,\dot{\varepsilon})}{RT}] + n(T)\ln[\sinh(\alpha\sigma_p)] \quad (3)$$

The values of n at each deformation temperature can be obtained from the slopes of the $\ln\dot{\varepsilon}$ - $\ln[\sinh(\alpha\sigma_p)]$ plots (Fig. 3a). By linear fitting, a good linear relationship between n and the deformation temperature is obtained (Fig. 3b), which is formulated in Eq. (4). The regression coefficients are presented in Table 2. It is evident that the n value decreases linearly with increasing temperature.

$$n = B_0 + B_1 T \quad (4)$$

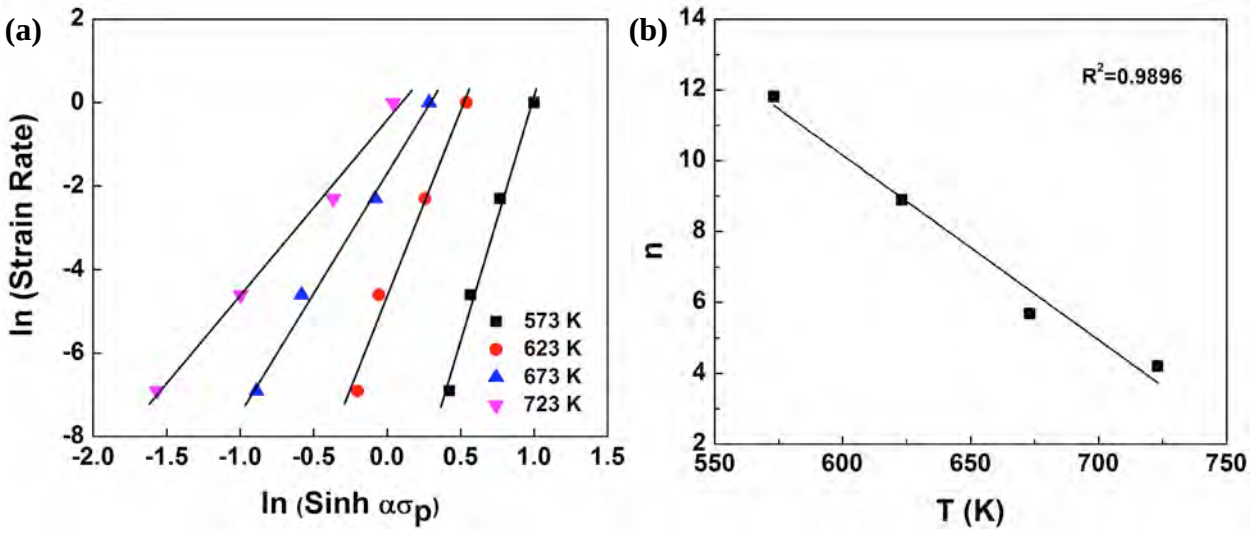

Fig. 3. Relationships between (a) $\ln\dot{\varepsilon}$ and $\ln[\sinh(\alpha\sigma_p)]$ and (b) n and T.

At a constant strain rate, the partial differentiation of Eq. (2) yields [22],

$$Q(T,\dot{\varepsilon}) = Rn(T)[\frac{\partial \ln[\sinh(\alpha\sigma_p)]}{\partial(1/T)}]_{\dot{\varepsilon}} = Rn(T)S(\dot{\varepsilon}) \quad (5)$$

Based on the measured true stress-true strain data, the values of S at each of the strain rates can be determined from the slopes of the $\ln[\sinh(\alpha\sigma_p)]$ - $1/T$ plots (Fig. 4a). From regression fitting, an excellent polynomial relationship between S and strain rate is found (Fig. 4b), as expressed in Eq. (6). The regression coefficients in Eq. (4) and (6) for all seven alloys studied are listed in Table 2. Based on the obtained $n(T)$ and $S(\dot{\varepsilon})$ functions, the activation energy $Q(T,\dot{\varepsilon})$ can be evaluated in Eq. (7).

$$S = C_0 + C_1(\ln\dot{\varepsilon}) + C_2(\ln\dot{\varepsilon})^2 \quad (6)$$

$$Q = R[B_0C_0 + C_0B_1T + B_1C_1T(\ln\dot{\varepsilon}) + B_1C_2T(\ln\dot{\varepsilon})^2 + B_0C_1(\ln\dot{\varepsilon}) + B_0C_2(\ln\dot{\varepsilon})^2] \quad (7)$$

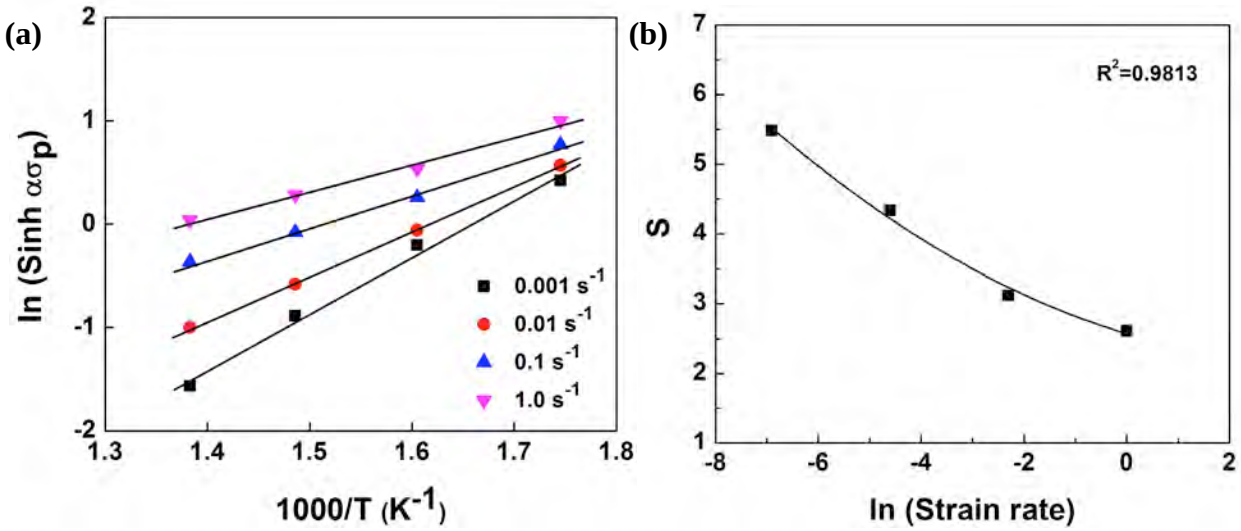

Fig. 4. Relationships between (a) $\ln[\sinh(\alpha\sigma_p)]$ and $1000/T$ and (b) S and $\ln\dot{\varepsilon}$.

Table 2 Regression Coefficients in Eq. (4) and (6) for all the alloys studied.

Alloy	Coefficients				
	B_0	B_1	C_0	C_1	C_2
Base alloy	36.7633	-0.0458	2.5470	-0.2333	0.0311
With 0.04%Zr	35.6321	-0.0441	2.4445	-0.2563	0.0287
With 0.12%Zr	38.6952	-0.0481	2.7432	-0.0884	0.0509
With 0.15%Zr	41.4529	-0.0521	2.5739	-0.2175	0.0303
With 0.05%V	43.7779	-0.0555	2.8703	-0.2573	0.0250
With 0.11%V	33.0255	-0.0399	2.9322	-0.2866	0.0091
With 0.15%V	31.7604	-0.0380	3.1248	-0.4438	-0.0197

By substituting the values of n at each deformation temperature and S at each strain rate into Eq. (5). the evolution of Q (the activation energy map) of the alloy with 0.15% Zr can be generated (Fig. 5). The predicted values of Q derived from Eq. (7) are also shown in Fig. 6(d), which demonstrate excellent agreement with those obtained from the experimental data (Fig. 5). It is evident that the

activation energy for hot deformation decreases with increasing temperature and strain rate, where it reaches 540 kJ/mol at 573 K and 0.001 s^{-1}, whereas declines by 83% (90 kJ/mol) at 723 K and 1 s^{-1}, indicating decreasing deformation resistance as the temperature and the strain rate increase. The results in Fig. 5 and 6(d) reveal that the activation energy for hot deformation should not be treated solely by a constant value, but considered as a function of deformation temperature and strain rate.

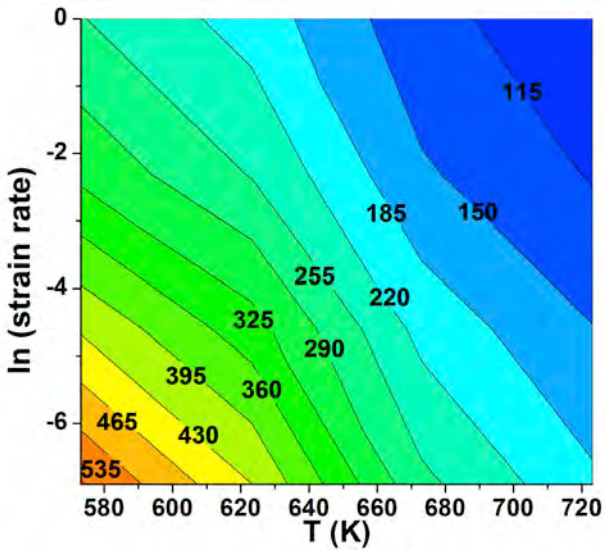

Fig. 5. Evolution of Q value (kJ/mol) as a function of deformation temperature and strain rate.

Furthermore, to verify the accuracy of the developed Q equation (Eq. (7)), the error between the predicted activation energy (Q_p) and the calculated value from experimental data (Q_M) can be estimated by:

$$error\% = \left| \frac{Q_p - Q_M}{Q_M} \right| \times 100 \tag{8}$$

The mean error for the alloy containing 0.15% Zr under various deformation conditions studied is determined to be 4.36%, which indicates good agreement between the predicted and measured activation energies.

Likewise, the material variables n and s for other six alloys are calculated according to Eq. (2), (3) and (5), and display excellent linear relationships with T and polynomial relationships with $\dot{\varepsilon}$ respectively. Consequently, the activation energy maps of the base alloy and the alloys containing 0.04-0.15% Zr and 0.05-0.15% V are generated (Fig. 6). Furthermore, in an attempt to gain more insight into the effect of micro-alloying of Zr and V on the activation energy at various working conditions, the variations in activation energy value as a function of deformation temperature and strain rate are shown in Fig. 7 and 8.

In general, the activation energies for hot deformation of all 7150 alloys are quite sensitive to the deformation conditions, and decrease with increasing deformation temperature and strain rate (Fig. 6-8), indicating that plastic deformation occurs more easily as the temperature and strain rate increase.

Besides, a higher decline rate in activation energy with increasing temperature exhibits during the deformation at a lower strain rate.

When the material is alloyed with 0.04% Zr (Fig. 6b), the alloy exhibits a similar activation energy map to the base alloy (Fig. 6a). The comparable values of activation energy are observed in both maps under any given deformation condition. With increasing Zr content from 0.12% to 0.15%, the levels of activation energy generally increase at most deformation conditions compared to the base alloy (Fig. 6c and d). For example, under the deformation condition at 573 K and 0.001 s^{-1}, the activation energy of the base alloy is 500 kJ/mol, which increases to 520 kJ/mol and 540 kJ/mol respectively, by the additions of 0.12% and 0.15% Zr. As the deformation temperature increases to 673 K and the strain rate increases to 1 s^{-1}, the activation energies of the alloys containing 0.12% and 0.15% Zr increase to 137 kJ/mol and 142 kJ/mol respectively, representing 21.4% and 25.7% increases relative to the base alloy. Moreover, Fig. 7 reveals that, at all constant strain rates, the increments of activation energy at lower deformation temperatures are remarkably higher than those at higher deformation temperatures due to the Zr addition. Toward higher deformation temperature (723 K), the values of activation energy of the base alloy and the alloys containing Zr become much closer. These results indicate that micro-alloying with a Zr content greater than 0.04% increases the deformation resistance during hot deformation preferentially at low deformation temperatures.

On the other hand, the alloy containing 0.05% V shows higher values of activation energy at any given deformation condition relative to the base alloy (Fig. 6e), and the dramatic rise in activation energy is observed at lower deformation temperatures between 573 and 623 K (Fig. 8), indicating a high degree of deformation difficulty as the temperature decreases. The further addition of 0.11% and 0.15% V also generally increases activation energies under the majority of deformation conditions (Fig. 6f and g). Particularly, at higher strain rates (0.1-1 s^{-1}), no significant decrease in the increment of activation energy is observed with increasing deformation temperature, indicating an enhanced deformation resistance at high temperatures due to the V addition (Fig. 8), which is different from the results observed in the alloys with Zr addition (Fig. 7). However, the activation energies are observed lower than those of the base alloy (Fig. 8c and d) when the deformation was performed at lower deformation temperatures (573-700 K) and at low strain rates (0.001 and 0.008 s^{-1}), as indicated by the shadow region in Fig. 6f and g, which suggests easier conduction of deformation under those conditions for alloys containing 0.11% and 0.15% V.

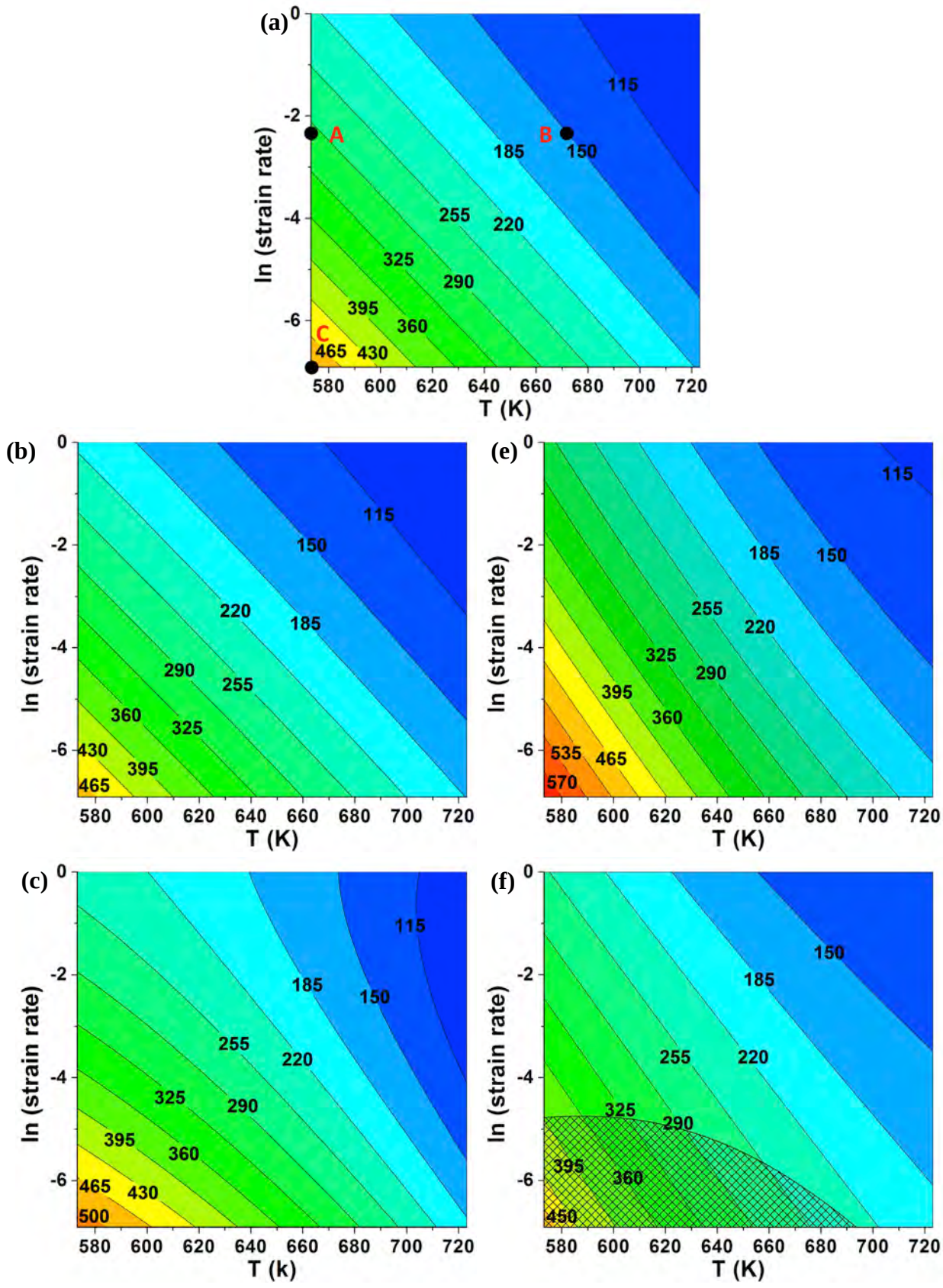
(a)
ln (strain rate)
T (K)
A
B
C
115
150
185
220
255
290
325
360
395
430
465
(b)
ln (strain rate)
T (K)
115
150
185
220
255
290
325
360
395
430
465
(e)
ln (strain rate)
T (K)
115
150
185
220
255
290
325
360
395
465
535
570
(c)
ln (strain rate)
T (k)
115
150
185
220
255
290
325
360
395
430
465
500
(f)
ln (strain rate)
T (K)
150
185
220
255
290
325
360
395
450

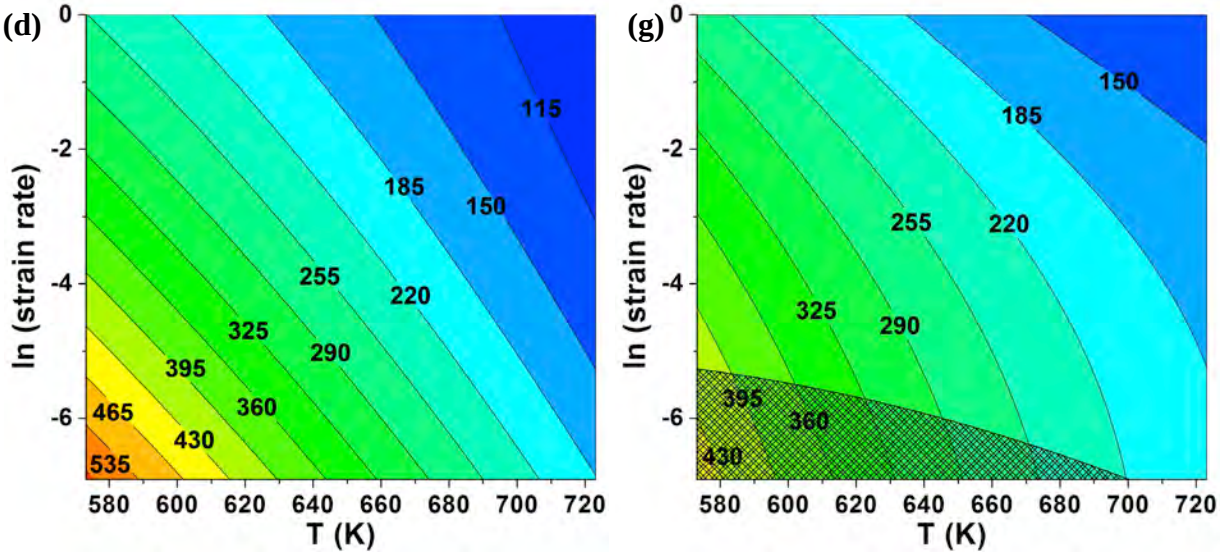

Fig. 6. Evolution of activation energy Q map for hot deformation of (a) the base alloy; and the alloys with (b) 0.04% Zr, (c) 0.12% Zr, (d) 0.15% Zr, (e) 0.05%V, (f) 0.11% V, and (g) 0.15% V.

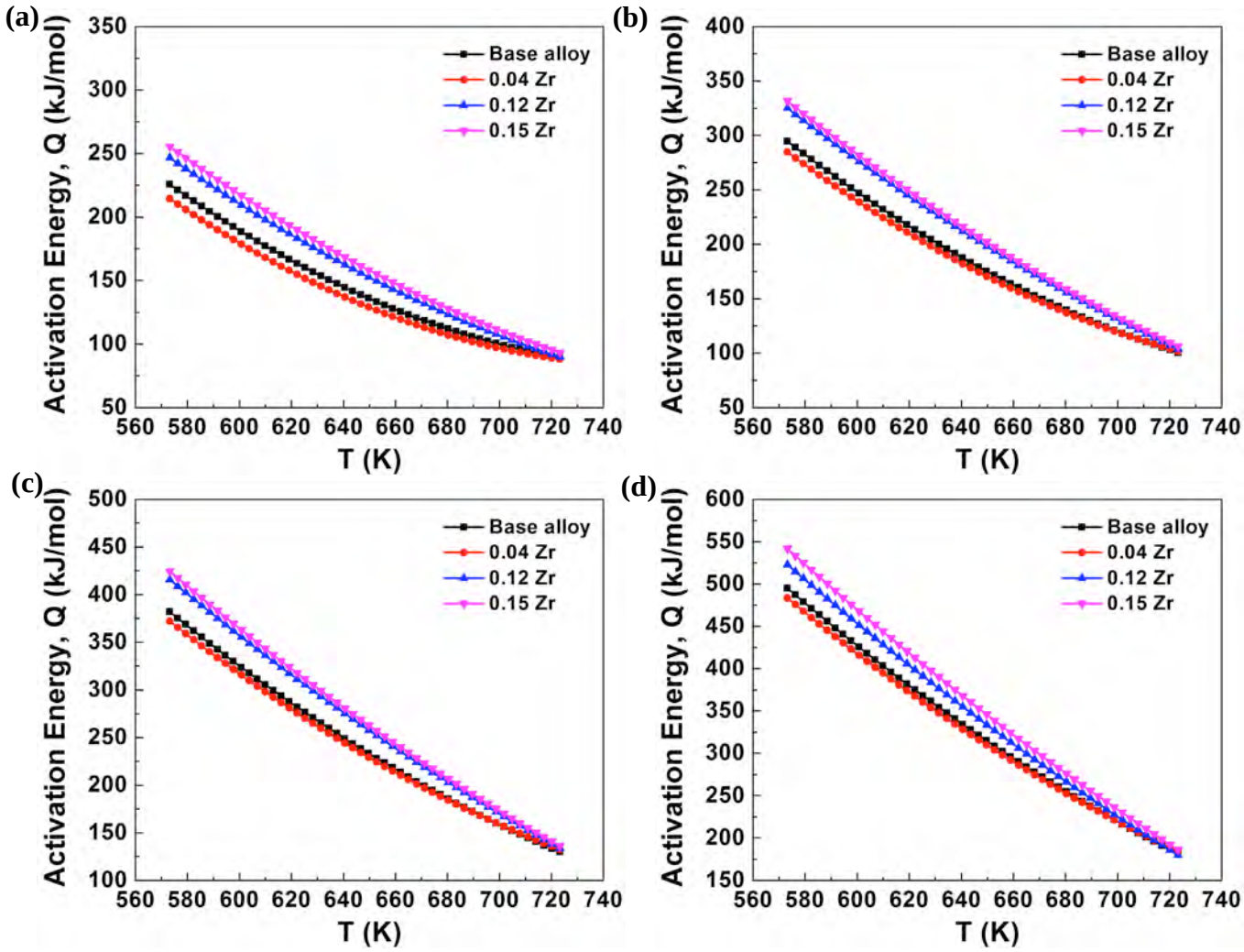

Fig. 7. Evolution of activation energies of the 7150 alloys containing different Zr contents with deformation temperature at the strain rates of (a) 1 s^{-1}, (b) 0.1 s^{-1}, (c) 0.01 s^{-1}, and (d) 0.001 s^{-1}.

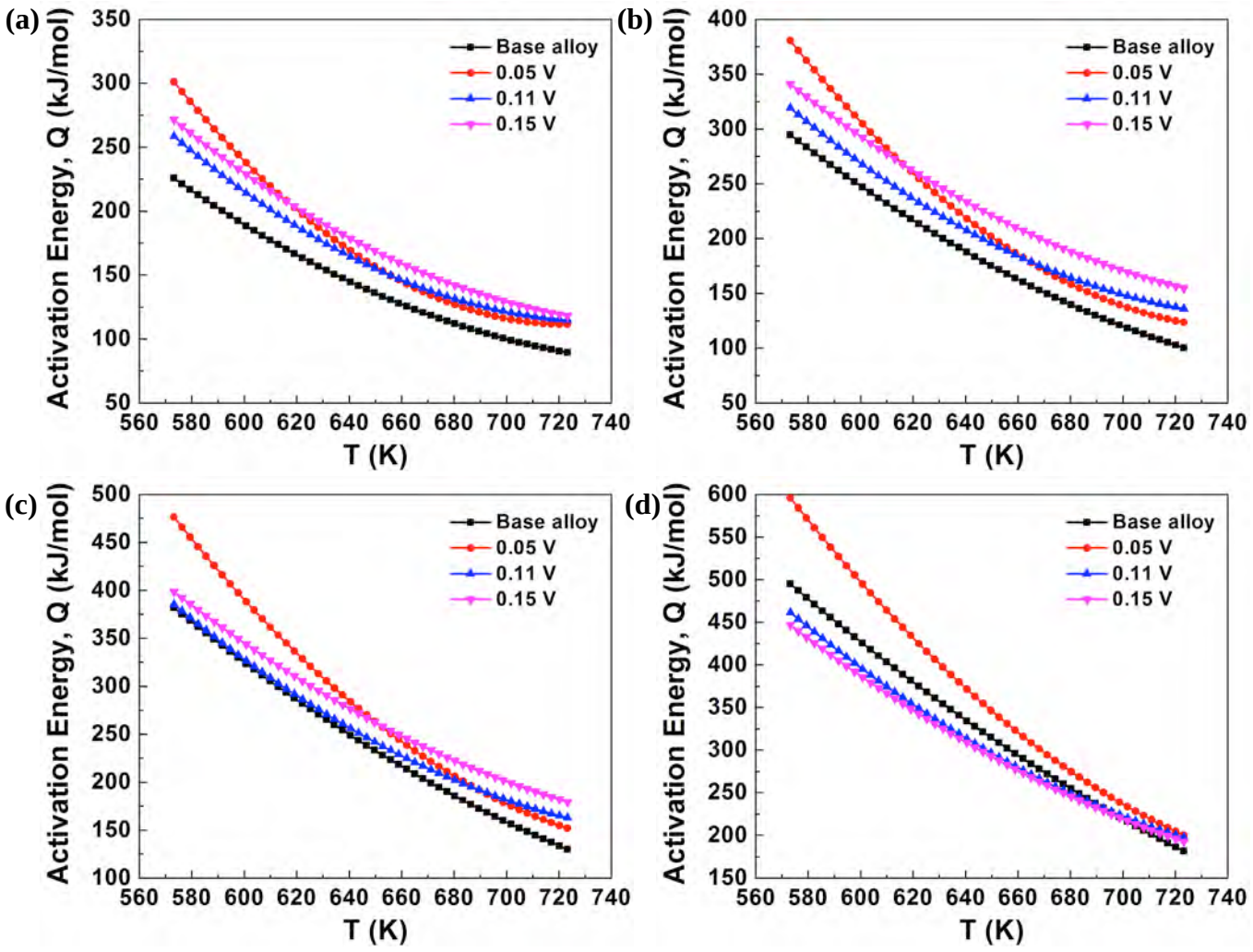

Fig. 8. Evolution of activation energies of the 7150 alloys containing different V contents with deformation temperature at the strain rates of (a) 1 s^{-1}, (b) 0.1 s^{-1}, (c) 0.01 s^{-1}, and (d) 0.001 s^{-1}.

3.3 Microstructure characterization

Initial microstructure after homogenization heat treatment

The microstructure evolution of the 7150 alloys with Zr additions from 0 to 0.15% and those with V additions from 0.01 to 0.15% after homogenization has been reported in our previous studies [19,20]. The homogenized structures of all alloys are composed of uniform equiaxed grains. After homogenization at 738 K for 24 h, the precipitation of fine Al_3Zr dispersoids is found in the alloys containing 0.12 and 0.15% Zr. Fig. 9a shows a number of spheroidal and coherent Al_3Zr dispersoids with an average diameter of 15 nm precipitated in the alloy with 0.12% Zr. When the added V ranges between 0.11 and 0.15%, the precipitation of incoherent V-containing dispersoids is clearly observed in the microstructure, which were identified as $Al_{21}V_2$-type phase by TEM selected area electron diffraction [28]. Fig. 9b shows that a large amount of spheroidal $Al_{21}V_2$ dispersoids with an average diameter of 51 nm are precipitated in the alloy containing 0.11% V. In the alloys with lower contents of

Zr (0.04%) and V (0.05%), almost no Al_3Zr and $Al_{21}V_2$ dispersoids are observed, indicating that the added Zr and V at those low levels mainly exist as the solute atoms in the aluminum matrix.

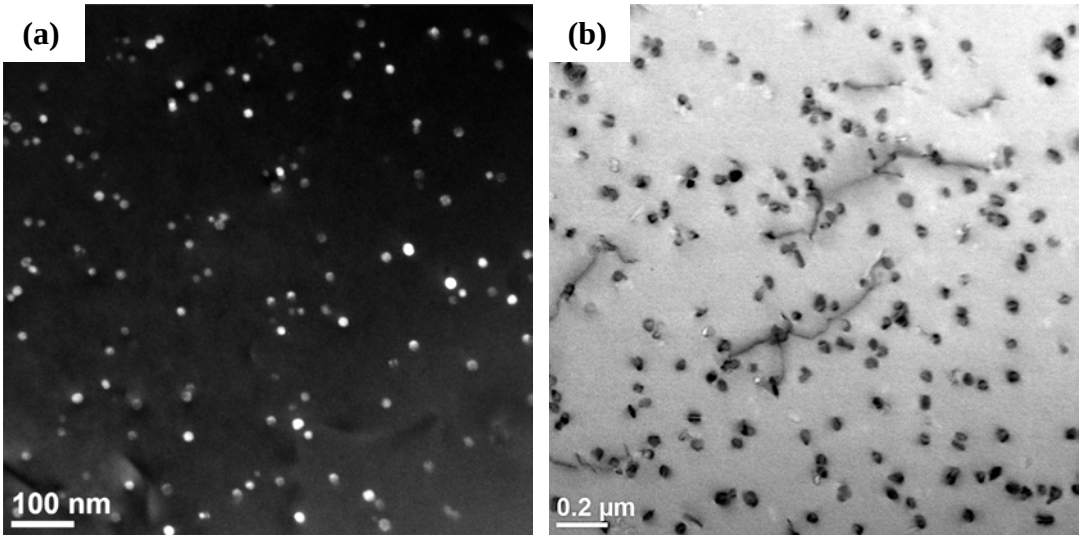

Fig. 9. The precipitation of Al_3Zr and $Al_{21}V_2$ dispersoids in as-homogenized samples: (a) Dark-field TEM micrograph showing Al_3Zr dispersoids in alloy with 0.12% Zr; and (b) STEM image displaying $Al_{21}V_2$ dispersoids in alloy with 0.11% V.

Deformed microstructure after hot compression

To understand the effect of Zr and V additions on the activation energy map for 7150 alloys, the deformed microstructures of the base alloy and the alloys containing 0.12% Zr, 0.05% V and 0.11% V under three selected deformation conditions (indicated as A, B and C in Fig. 6a) were investigated using the EBSD and TEM techniques. Conditions A and B represent the deformation conditions at which the activation energies are increased due to the micro-alloying of Zr and V. At Condition C, the alloys containing 0.12% Zr and 0.05% V display remarkable increases in activation energy, whereas the alloy with 0.11% V shows a lower value of activation energy compared with the base alloy. In EBSD analysis, the boundary misorientation angles can be distinguished as follows: white lines: 1-5°; blue lines: 5-15°; thin black lines: 15-30° and thick black lines: (> 30°).

When the deformation is conducted at 573 K and 0.1 s^{-1} (Condition A), a large number of low-angle subgrain boundaries of 1-5° are observed inside the elongated grains of the four alloys (Fig. 10a-d). Compared to the base alloy, the deformation of the alloys containing Zr and V becomes heterogeneous associated with the formation of irregular deformation bands (Fig. 10b-d). As the deformation temperature increases to 673 K at the same strain rate of 0.1 s^{-1} (Condition B), the deformation of all four alloys becomes more homogeneous, and the recovered substructures become better organized with larger subgrains (Fig. 10e-h). This is consistent with our previous observations during hot deformation of 7150 alloys [19,20,26], in which the level of dynamic recovery is increased with increasing temperature and decreasing strain rate. It is evident that the base alloy displays a high level of dynamic recovery with a number of subgrains characterized by higher angle boundaries (5-15°) (Fig. 10e). However, the low-angle boundaries of 1-5° are mainly observed in recovered structures of the alloys

containing Zr and V (Fig. 10f-h), indicating a restrained dynamic recovery. Hence, as the deformation temperature increases, the improved dynamic recovery leads to the decrease in dislocation density and facilitation of further dislocation motion [2,7], thus, substantially reduces the resistance to dislocation slipping and decrease the activation energy for hot deformation (Fig. 6). Conversely, the decreased level of dynamic recovery due to the Zr and V additions results in the increase of activation energy compared to the base alloy, as observed in Fig. 6.

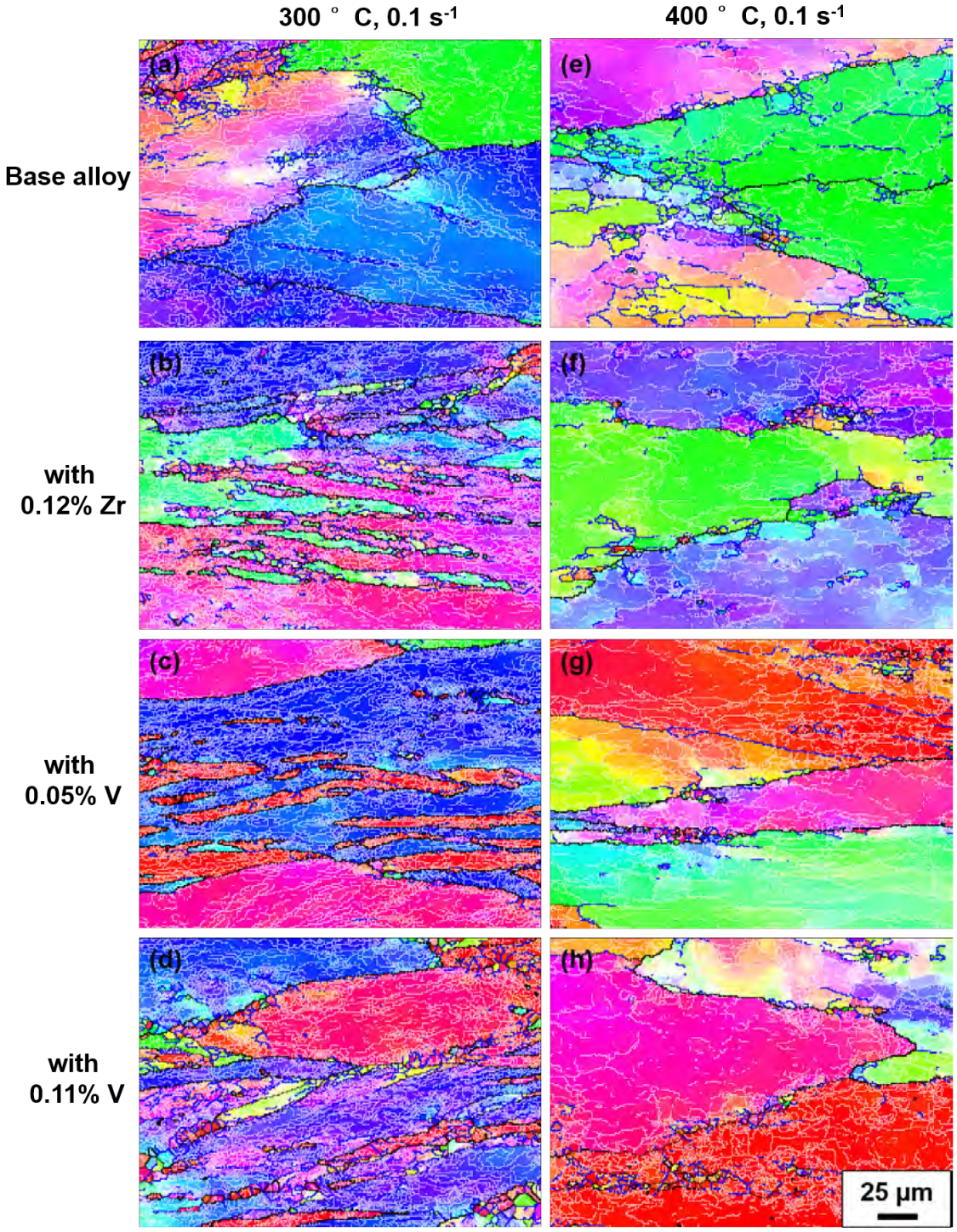

Fig. 10. Orientation imaging maps of the base alloy and the alloys with 0.12% Zr, 0.05%V and 0.11% V under deformation conditions of A and B as illustrated in Fig. 6a.

Moreover, under the deformation condition at the low temperature of 573 K and low strain rate of 0.001 s^{-1} (Condition C), the dynamic precipitation is clearly observed in the deformed microstructures of all the 7150 alloys studied, and these precipitates are identified as $Mg(Zn,Cu)_2$ phase [26]. STEM micrographs in Fig. 11 show that the $Mg(Zn,Cu)_2$ precipitates are rather coarse and have similar average diameters of 97, 93, 95 and 101 nm in the samples of the base alloy and the alloys with 0.12% Zr, 0.05% V and 0.11% V respectively. The variations in the volume fraction of precipitates due to the microalloying of Zr and V are illustrated in Fig. 12. The volume fraction of precipitates in the base alloy is determined to be 8.5%, while the alloys containing 0.12% Zr and 0.05% V exhibit comparable levels of precipitation, being 8.6% and 8.4% respectively. However, the amount of precipitates in the alloy with 0.11% V rises up to 12.2%, representing a 44% increase relative to that in the base alloy, which indicates a strong dynamic precipitation with 0.11% V addition. It has been reported that the high-energy incoherent interfaces between the $Al_{21}V_2$ dispersoids and the aluminum matrix likely provide efficient heterogeneous nucleation sites for the dynamic precipitation of $Mg(Zn,Cu)_2$, thereby leading to an increase of precipitate density with 0.11% V addition [29-31]. On the contrary, the coherent Al_3Zr dispersoids and the V solutes in the alloys with 0.12% Zr and 0.05% V do not have effect on the dynamic precipitation, associated with a similar volume fraction of $Mg(Zn,Cu)_2$ precipitates relative to the base alloy. McQueen and other researchers [2,15,32,33] reported that dynamic precipitation and precipitate coarsening during deformation of aluminum alloys resulted in a poor pinning effect on dislocation mobility and a weak solute drag effect due to the depletion of solutes, thus leading to a decrease of the deformation resistance. Therefore, during the deformation at low temperatures and low strain rates, the reduction of activation energies in the alloy with 0.11% V relative to the base alloy (Fig. 6f and 8d) is attributed to the enhanced dynamic precipitation of coarse $Mg(Zn,Cu)_2$ precipitates accompanied by severe depletion of solutes.

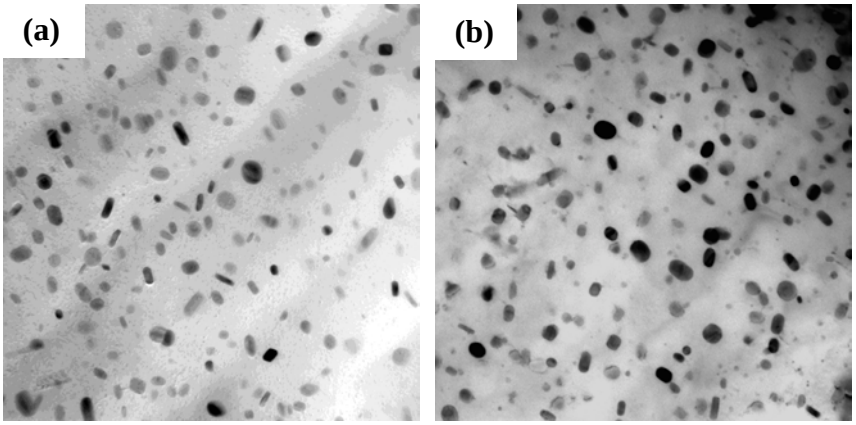

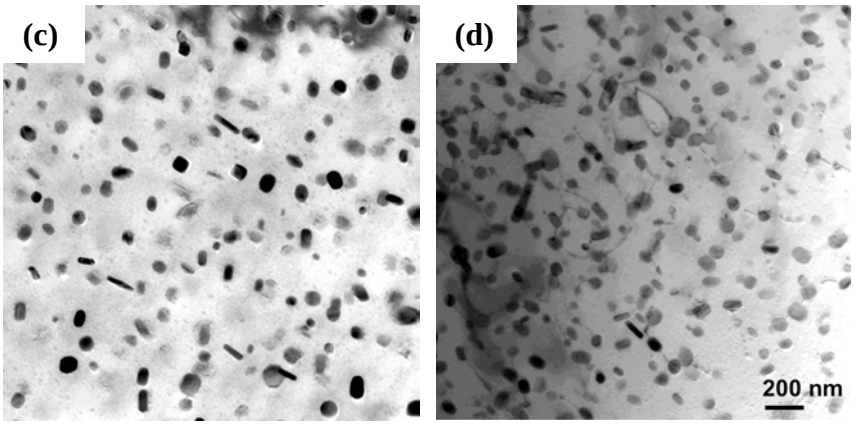

Fig. 11. STEM images showing the dynamic precipitation of $Mg(Zn,Cu)_2$ in the samples deformed at 573 K and $0.001s^{-1}$ (Condition C in Fig. 6a): (a) base alloy and the alloys with (b) 0.12% Zr, (c) 0.05% V, and (d) 0.11% V.

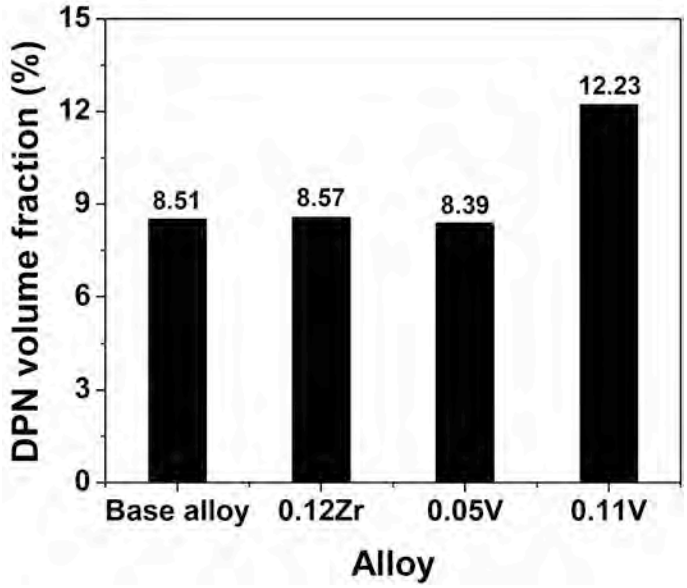

Fig. 12. Volume fractions of dynamic precipitation of $Mg(Zn,Cu)_2$ as a function of Zr and V contents.

4. Discussion

The activation energy *Q* maps for hot deformation of 7150 aluminum alloys with Zr additions ranging from 0 to 0.15% and V additions ranging from 0.01 to 0.15% were generated based on the revised Sellars' constitutive equation (Eq. 2). The results reveal that the activation energy varies with deformation temperature, strain rate and addition of alloying elements (Fig. 6-8). This is closely correlated with the thermodynamic mechanism of dislocation slipping during plastic deformation. Dislocations can move randomly when the energy barrier, i.e., an activation energy, is overcome (Fig. 13a), which is a thermally activated process [21]. When an external shear stress is applied in the direction of slip on the slip plane (Fig. 13b), the thermal energy needed to overcome the energy barrier for dislocations that are free to move is reduced [21,34]. Moreover, the dynamic restoration can reduce the dislocation density to facilitate further dislocation movement [7], thus decreasing the energy barrier

(activation energy) to dislocation motion (Fig. 13b). Conversely, the dislocation slip is hindered when the dislocation encounters the pile-up of dislocations, solute atoms and dispersive precipitates due to the dislocation interaction, solute drag and precipitate pinning effects. Thus, an increased activation energy is needed for the dislocation to overcome these obstacles [2,21], as illustrated in Fig. 13c. Based on the above knowledge, the evolution of activation energies of the 7150 alloys micro-alloyed with Zr and V under different deformation conditions will be discussed in the following sections.

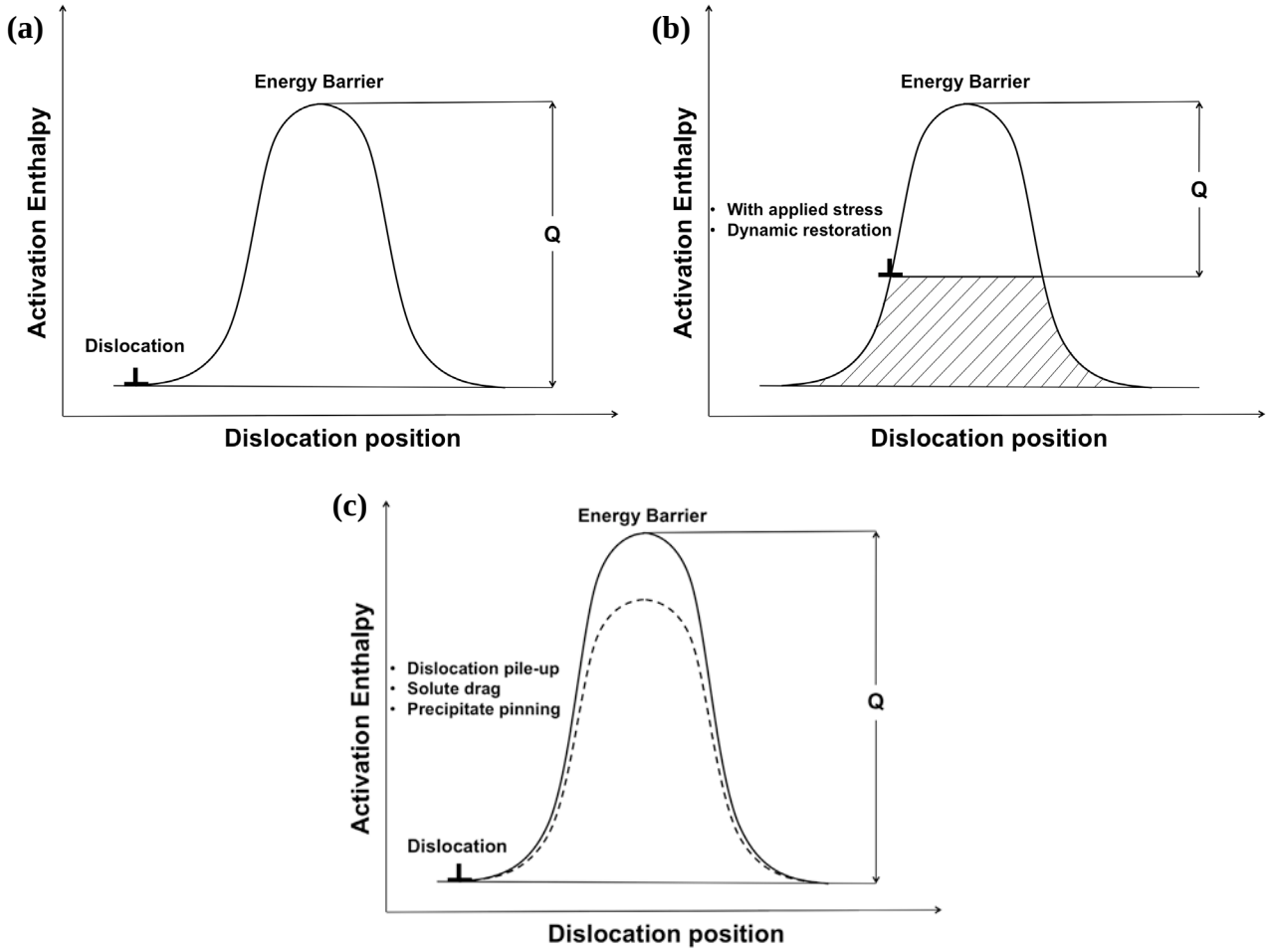

Fig. 13. Schematic illustration of evolution of activation energy for dislocation motion: (a) only by thermal activation, (b) with applied stress and dynamic restoration assistance (a reduced Q) and (c) with the presence of dislocation pile-up, solute atoms and precipitates in the microstructure (an increased Q).

4.1 Effects of deformation temperature and strain rate on activation energy maps

The activation energies for hot deformation of all 7150 alloys were generally observed to decrease with increasing temperature and increasing strain rate (Fig. 6). Thermal activation, which favors overcoming the energy barrier to dislocation motion, increases with increasing temperature [21]. In addition, the level of dynamic recovery is increased as the temperature increases (Fig. 9). Hence, the increase of deformation temperature could substantially decrease the activation energy for hot

deformation due to the increased thermal activation and improved dynamic recovery. On the other hand, with increasing strain rate, the applied external force increases and leads to an augmented shear stress to activate the motion of dislocations [21,34]. Besides, the dislocation multiplication rate increases with increasing strain rate, thereby resulting in an increase in the rate of dynamic recovery [2,7,34]. Therefore, both factors attribute to the decrease in activation energy.

Moreover, a higher decline rate in activation energy with increasing temperature is observed during the deformation at a lower strain rate (Fig. 6). At higher strain rates, the applied shear stress can largely reduce the energy barrier, and then the dislocation can move with much less thermal activation, indicating a deceasing dependency of deformation on temperature. However, due to a decrease in shear stress at lower strain rates, the dislocation slip occurs more dependent on the thermal activation. The increasing temperature can significantly improve the thermal activation and dynamic recovery, and thus remarkably decreases the activation energy, which is represented by a higher decline rate in activation energy at lower strain rates.

4.2 Effects of Zr and V on hot activation energy maps

When the material is alloyed with Zr from 0.12 to 0.15%, the activation energies for hot deformation are generally increased compared with the base alloy at all deformation conditions (Fig. 6 and 7). The addition of Zr results in the precipitation of a large number of Al_3Zr dispersoids during homogenization (Fig. 9a), which promote the pinning effect on the dislocation movement and retardation of dynamic recovery (Fig. 10), thereby leading to an increase of activation energies (Fig. 7). Similarly, for the alloys containing $Al_{21}V_2$ dispersoids (0.11-0.15% V), the activation energies are observed higher than those in the base alloy at the majority of deformation conditions (Fig. 6 and 8), which is attributed to the improved deformation resistance caused by the pinning effect by $Al_{21}V_2$ dispersoids.

Moreover, the increment of activation energy due to the Zr addition (0.12-0.15%) become lower with increasing deformation temperature at any constant strain rate (Fig. 7), which is the result of the improved thermal activation of dislocation motion and the increased level of dynamic recovery as the temperature increases. However, when the deformation is conducted at higher strain rates of 0.1-1 s^{-1}, no significant drop in the increment of activation energy with increasing deformation temperature is observed in the alloys containing V (0.11-0.15% V) relative to the base alloy (Fig. 8), showing an enhanced resistance to deformation at elevated temperatures. Our previous studies [19,20] suggested that with the same addition amount of Zr and V, the alloys containing V exhibit an even lower level of dynamic recovery compared to the alloys containing Zr, associated with the decreases in subgrain size and mean misorientation angles of boundaries at the same deformation condition. Hence, V alloying implies a higher dispersoid strengthening and a stronger restriction of dynamic softening, which may retain a high level of activation energy at elevated temperatures.

Nevertheless, remarkable decreases in activation energy exhibit in the alloys with 0.11-0.15% V compared to the base alloy at low temperatures of 573-700 K with low strain rates of 0.001-0.008 s^{-1} (Fig. 6a, f and g). During slow deformation at lower temperatures, the $Mg(Zn,Cu)_2$ phase is dynamically precipitated and become coarsening in homogenized 7150 alloys, as shown in Fig. 11.

When 0.11-0.15% V are added, the dynamic precipitation is improved with a remarkable increase of the amount of coarse $Mg(Zn,Cu)_2$ precipitates (Figs. 11d and 12). Thus, the enhanced dynamic precipitation and severe depletion of solutes in the alloys with 0.11-0.15% V that offset the $Al_{21}V_2$ dispersoid pinning effect lead to the decreased deformation resistance and activation energies at low deformation temperatures and low strain rates. On the other hand, the alloys containing 0.12-0.15% Zr and 0.05% V present similar volume fractions of $Mg(Zn,Cu)_2$ precipitates relative to the base alloy, still displaying strong Al_3Zr dispersoid pinning and V solute drag effects under those deformation conditions.

At a lower V level of 0.05% in which V mainly exists as solutes in the aluminum matrix, the alloy displays significant increases in activation energy compared with the base alloy, particularly at lower temperatures (573-623 K) (Fig. 6e and 8). This is correlated with the V solute drag effect on dislocation slip and the restrained dynamic recovery as shown in Fig. 10c and g, leading to an enhanced deformation resistance. Due to a decrease in diffusion rate of vanadium in aluminum matrix with decreasing temperature, the strengthening effect by the V solutes is more prominent as the temperature decreases [20], resulting in the significant increases in activation energy at lower temperatures (Fig. 8). However, no significant change in the activation energy map is observed between the 7150 base alloy and the alloy containing 0.04% Zr in solution (Fig. 6a, b and Fig. 7), which is because of the higher diffusivity of zirconium solutes in aluminum [35], resulting in weaker solute drag effect.

The present study demonstrates that the activation energy map for hot deformation can not only describe the thermomechanical dependency of the activation energy for each alloy, but also reveal more valuable technical details on the hot workability under various deformation conditions, which could not be addressed solely based on a constant value of the activation energy for a given material. By comparing the activation energy maps over all deformation conditions for the alloys studied, the effects of microalloying of Zr and V on the plastic deformation of 7150 alloys under specific deformation conditions are better discovered. Therefore, the activation energy map may provide a powerful tool for optimizing the hot working processes of aluminum alloys.

5. Conclusions

1. Using a revised Sellars' constitutive equation, the activation energy maps for hot deformation of 7150 alloys are proposed, which are considered as a function of deformation temperature, strain rate and micro-alloying elements.
2. The activation energies for hot deformation of the alloy with 0.12-0.15% Zr are remarkably increased compared to those of the base alloy at most deformation conditions, due to the pinning effect of Al_3Zr dispersoids on dislocation and the restrained dynamic recovery.
3. The 0.05% V addition significantly increases activation energies, preferentially at lower temperatures of 573-623 K, correlated to a strong solute drag effect of V atoms.
4. At higher V additions from 0.11 to 0.15%, the activation energy generally increases at the majority of deformation conditions due to $Al_{21}V_2$ dispersoid pinning effect. Remarkable decreases in activation energy exhibit at low deformation temperatures of 573-700 K and at low strain rates of 0.001-0.008 s^{-1}, attributed to the enhanced dynamical precipitation of $Mg(Zn,Cu)_2$ and severe

depletion of solutes.

5. The activation energy map can provide valuable technical information on the hot workability under various deformation conditions for a given alloy. By comparing the activation energy maps for the alloys studied, the effects of microalloying of Zr and V on the plastic deformation of 7150 alloys under specific deformation conditions are better understood.

Acknowledgments

The authors would like to acknowledge the financial support from the Natural Sciences and Engineering Research Council of Canada (NSERC) and from Rio Tinto Alcan through the NSERC Industrial Research Chair in Metallurgy of Aluminum Transformation at the University of Québec at Chicoutimi. The authors would also like to thank Ms. E. Brideau for her assistance in the hot compression tests performed on the Gleeble 3800 thermomechanical simulator.

References

[1] E.A. Starke, J.T. Staley, Prog. Aerosp. Sci. 32 (1996) 131-172.

[2] H.J. McQueen, S. Spigarelli, M. Kassner, E. Evangelista, Hot Deformation and Processing of Aluminum Alloys, CRC Press, Florida, 2011, pp. 87-233.

[3] E. Cerri, E. Evangelista, H.J. McQueen, High Temp. Mat. Proc. 18 (1999) 227-240.

[4] J.D. Robson, Acta Mater. 52 (2004) 1409-1421.

[5] S. Hirosawa, T. Sato, A. Kamio, H.M. Flower, Acta Mater. 48 (2000) 1797-1806.

[6] G.B. Schaffer, S.H. Huo, J. Drennan, G.J. Auchterlonie, Acta Mater. 49 (2001) 2671-2678.

[7] F.J. Humphreys, M. Hatherly, Recrystallization and Related Annealing Phenomena, second ed., Elsevier Ltd., Oxford, 2004, pp. 169-450.

[8] J.D. Robson, P.B. Prangnell, Acta Mater. 49 (2001) 599-613.

[9] Y.V. Milman, A.I. Sirko, D.V. Lotsko, D.B. Miracle, O.N. Senkov, Mater. Sci Forum 396-402 (2002) 1217-1222.

[10] E.F. Kazakova, Y.I. Rusnyak, Met. Sci. Heat Treat. 51 (2009) 436-439.

[11] K.E. Knipling, D.C. Dunand, D.N. Seidman, Z. Metallkd. 97 (2006) 246-265.

[12] J.R. Davis, ASM Specialty Handbook: Aluminum and Aluminum Alloys, American Society for Metals, Metals Park, OH, USA, 1993, pp. 23-58.

[13] Y. Lin, X. Chen, Mater. Des. 32 (2011) 1733-1759.

[14] C.M. Sellars, W.J. McTegart, Mem. Sci. Rev. Met. 63 (1966) 731-746.

[15] E. Cerri, E. Evangelista, A. Forcellese, Mater. Sci. Eng. A 197 (1995) 181-198.

[16] N. Jin, H. Zhang, Y. Han, W. Wu, J. Chen, Mater. Charact. 60 (2009) 530-536.

[17] T. Sheppard, A. Jackson, Mater. Sci. Technol. 13 (1997) 203-209.

[18] H. Hu, L. Zhen, L. Yang, W. Shao, B. Zhang, Mater. Sci. Eng. A 488 (2008) 64-71.

[19] C. Shi, X.-G. Chen, Mater. Sci. Eng. A 596 (2014) 183-193.

[20] C. Shi, X.-G. Chen, Mater. Sci. Eng. A 613 (2014) 91-102.

[21] D. Caillard, J.L. Martin, Thermally Activated Mechanisms in Crystal Plasticity, Pergamon Press, Oxford, 2003, pp. 1-280.

[22] C. Shi, W. Mao, X.-G. Chen, Mater. Sci. Eng. A 571(2013) 83-91.

[23] P.M. Kelly, Met. Forum 5 (1982) 13-23.

[24] O.D Sherby, J.L Lytton, J.E Dorn, Acta Metall. 5 (1957) 219-227.

[25] R.W. Lund, W.D. Nix, Metall. Trans. A 6 (1975) 1329-1333.

C. Shi, X.-G. Chen, Effects of Zr and V microalloying on activation energy during hot deformation of 7150 alloys, Light Metals 215, ed. M. Hyland, TMS 2015, p. 163-167

[26] C. Shi, J. Lai, X.-G. Chen, Materials 7 (2014) 244-264.

[27] A.M. Bunn, P. Schumacher, M.A. Kearns, C.B. Boothroyd, A.L. Greer, Mater. Sci. Technol. 15 (1999) 1115-1123.

[28] J. Lai, C. Shi, X. Chen, Mater. Charact. 96 (2014) 126-134.

[29] L.M. Wu, W.H. Wang, Y.F. Hsu, S. Trong, J. Alloys Comp. 456 (2008) 163-169.

[30] B.L. Ou, J.G. Yang, M.Y. Wei, Metall. Mater. Trans. A 38A (2007) 1760-1773.

[31] M. Conserva, E. Di Russo, and O. Caloni, Metall. Trans. 2 (1971) 1227-1232.

[32] X. Huang, H. Zhang, Y. Han, J. Chen, Mater. Sci. Eng. A 527 (2010) 485-490.

[33] S.Y. Chen, K.H. Chen, G.S. Peng, X.H. Chen, Q.H. Cheng, J. Alloys Comp. 537 (2012) 338-345.

[34] R.W.K. Honeycombe, The plastic deformation of metals, second ed., Edward Arnold Ltd. Maryland, 1984, pp. 33-128.

[35] G. Neumann, C. Tuijn, Self-diffusion and Impurity Diffusion in Pure Metals: Handbook of Experimental Data, Elsevier Ltd., New York, 2009, pp. 121-148.